International Journal of Nanomedicine Dovepress

Open Access Full Text Article ORIGINAL RESEARCH

# The Cervical and Meningeal Lymphatic Network as a Pathway for Retrograde Nanoparticle Transport to the Brain

Héctor M Ramos-Zaldívar[1], Iva Polakovicova[2,3,†], Edison Salas-Huenuleo[4], Claudia P Yefi[5], David Silva-Ancahuail[2,6], Pedro Jara-Guajardo[2,6], Juan Esteban Oyarzún[7,8], Álvaro Neira-Troncoso[3,9], Patricia V Burgos[9], Viviana A Cavieres[9], Eloísa Arias-Muñoz[9], Carlos Martínez[10], Ana L Riveros[2,6], Alejandro H Corvalán[2,3], Marcelo J Kogan[2,6], Marcelo E Andia[7,8]

[1]Doctoral Program in Medical Sciences, Faculty of Medicine, Pontificia Universidad Católica de Chile, Santiago, Chile; [2]Advanced Center for Chronic Diseases (ACCDiS), Santiago, Chile; [3]Department of Hematology and Oncology, Faculty of Medicine, Pontificia Universidad Católica de Chile, Santiago, Chile; [4]Advanced Integrated Technologies SpA, (AINTECH), Santiago, Chile; [5]Escuela de Medicina Veterinaria, Facultad de Ciencias de la Naturaleza, Universidad San Sebastián, Santiago, Chile; [6]Departamento de Química Farmacológica y Toxicológica, Facultad de Ciencias Químicas y Farmacéuticas, Laboratorio de Nanobiotecnología, Universidad de Chile, Santiago, Chile; [7]Millennium Institute for Intelligent Healthcare Engineering, Santiago, Chile; [8]Biomedical Imaging Center, School of Medicine, Pontificia Universidad Católica de Chile, Santiago, Chile; [9]Centro de Biología Celular y Biomedicina (CEBICEM), Facultad de Medicina y Ciencia, Universidad San Sebastián, Santiago, Chile; [10]Experimental Surgery and Simulation Center, Department of Digestive Surgery, Clinic Hospital, School of Medicine, Pontificia Universidad Católica de Chile, Santiago, Chile

[†]Iva Polakovicova passed away on October 12, 2020

Correspondence: Héctor M Ramos-Zaldívar, Email hmramos@uc.cl



**Introduction:** The meningeal lymphatic vessels have been described as a pathway that transports cerebrospinal fluid and interstitial fluid in a unidirectional manner towards the deep cervical lymph nodes. However, these vessels exhibit anatomical and molecular characteristics typical of initial lymphatic vessels, with the absence of surrounding smooth muscle and few or absent valves. Given its structure, this network could theoretically allow for bidirectional motion. Nevertheless, it has not been assessed as a potential route for nanoparticles to travel from peripheral tissues to the brain.

**Methods:** We employed superparamagnetic iron oxide nanoparticles (SPIONs), exosomes loaded with SPIONs, gold nanorods, and Chinese ink nanoparticles. SPIONs were prepared via chemical coprecipitation, while exosomes were isolated from the B16F10 melanoma cell line through the Exo-Spin column protocol and loaded with SPIONs through electroporation. Gold nanorods were functionalized with polyethylene glycol. We utilized C57BL/6 mice for *post-mortem* and in vivo procedures. To evaluate the retrograde directional flow, we injected each nanoparticle solution in the deep cervical lymph node. The head and neck were fixed for magnetic resonance imaging and histological analysis.

**Results:** Here we show that extracellular vesicles derived from the B16F10 melanoma cell line, along with superparamagnetic iron oxide nanoparticles, gold nanorods, and Chinese ink nanoparticles can reach the meningeal lymphatic vessels and the brain of C57BL/6 mice after administration within the deep cervical lymph nodes *post-mortem* and in vivo, exclusively through lymphatic structures.

**Discussion:** The functional anatomy of dural lymphatics has been found to be conserved between mice and humans, suggesting that our findings may have significant implications for advancing targeted drug delivery systems using nanoparticles. Understanding the retrograde transport of nanoparticles through the meningeal lymphatic network could lead to novel therapeutic approaches in nanomedicine, offering new insights into fluid dynamics in both physiological and neuropathological contexts. Further research into this pathway may unlock new strategies for treating neurological diseases or enhancing drug delivery to the brain.

**Keywords:** extracellular vesicles, SPIONs, gold nanorods, Chinese ink, meningeal lymphatic vessels, nanomedicine

Received: 5 July 2024
Accepted: 5 October 2024
Published: 24 October 2024

# Introduction

The lymphatic system, including the meningeal lymphatic vessels, has usually been described as a unidirectional transport system of fluid and macromolecules from tissues to venous circulation.[1,2] This concept has prevented its examination as a nanoparticle and drug delivery pathway to the brain, as administered contents would be expected to all be cleared to the thorax. Nevertheless, evaluating nanoparticle flow through these vessels is relevant considering the participation of the lymphatic system in immune transportation, its pathologic involvement in cancer metastasis and the spreading of some infectious diseases, as well as its potential as a drug delivery pathway for its targeting and pharmacokinetic advantages, including bypassing first-pass metabolism in the liver.[3]

Studies in mice have described the anatomical and morphological characteristics of meningeal lymphatics to be consistent with initial lymphatic vessels.[4,5] This includes a noncontinuous basement membrane, sparse or no lymphatic valves, and no smooth muscle cell lining;[4,5] which implies that meningeal lymphatic vessels might not have a preferential flow determined by its own structural components. Together, these findings open a theoretical possibility for retrograde flow towards the brain that would depend on the physiological and mechanical conditions of the vessels.

Recent developments in the use of nanomaterials in lymphatic tissues have highlighted their potential as novel imaging agents, improving therapeutic targeting and enabling imaging-guided procedures.[6] This emphasizes the role that nanotechnology related to the cervical and meningeal lymphatic network could play in fields such as neuro-oncology and neuroimmunology.

Most cancer cells migrate through lymph nodes, and brain metastasis has a direct impact on survival.[7,8] These cells utilize extracellular vesicles for intercellular communication and the transportation of biological contents to guide the metastatic process and prepare the pre-metastatic niche.[7,9] Interestingly, extracellular vesicles have been found to move in a bidirectional manner between the brain parenchyma and peripheral tissues, although the underlying mechanisms and pathways remain poorly understood.[10] Despite this, retrograde flow through the cervical and meningeal lymphatic network has not been assessed to date.

The active involvement of immune cells within lymphatic vessels and the meninges further underscores the importance of this network in neuroimmunity.[11] Meningeal lymphatic vessels are integral to neuroimmune surveillance, draining central nervous system (CNS)-derived antigens to peripheral lymph nodes, where immune processing occurs.[11] Impairments in this system have been implicated in aging-related neurodegeneration, including conditions like Alzheimer's disease.[11] Additionally, in neuroinflammatory and autoimmune diseases such as multiple sclerosis, auto-reactive T cells infiltrate the CNS and cause neuronal damage.[11,12]

Here, we suggest that the cervical and meningeal lymphatic network can transport nanoparticles not only towards the thorax but can also serve to carry particles towards the brain.

# Materials and Methods

## Superparamagnetic Iron Oxide Nanoparticle Synthesis

Samples of iron oxide nanoparticles were prepared by a chemical coprecipitation process from $FeCl_3 \cdot 6H_2O$ (432 mg), and $FeCl_2 \cdot 4H_2O$ (159 mg). Ferric and ferrous chlorides were dissolved in 19mL of Milli-Q water with vigorous magnetic agitation at room temperature. One mL of ammonium (25%) was added to the solution with vigorous magnetic agitation for 10 min. Then, three washes with Milli-Q water were performed, maintaining iron-nanoparticles in an 80 mL beaker with a neodymium magnet. Subsequently, the superparamagnetic iron oxide nanoparticles were washed twice with nitric acid. Finally, iron-nanoparticles were dissolved in Milli-Q water for later characterization. A ten-fold stock dilution with Milli-Q water increased pH to 7.

## Characterization of Iron Oxide Nanoparticles

The morphology and particle size of SPIONs was investigated by scanning transmission electron microscopy (STEM, FEI Quanta 250) operating at 10.00 kV. The Malvern Zetasizer was used for dynamic light scattering size determination and superficial charge. The dynamic light scattering system was used to determine the size of nanoparticles at 25°C in Milli-Q water, with a detection angle of 173°. SPIONs were measured at a 1:10 dilution. SPIONs concentrations obtained

from the synthesis were measured using Nanoparticle Tracking Analysis by NanoSight. pH of the solutions was determined by pH meter. The concentration of iron nanoparticles in solutions was determined by inductively coupled plasma mass spectrometry (ICP MS).

## Cell Culture and Exosome Purification

The B16F10 (ATCC CRL-6475) melanoma cell line was cultured using Exo-free medium. The isolated supernatant was centrifuged twice: first at 300g for 10 min at 4 °C and then at 16000g for 20 min at 4 °C. Filtration followed through 0.2 μm pore size filters. For purification, an Exo-spin (CELL GS) protocol was conducted. Extracellular vesicles were first concentrated using a 10 kDa filter to separate larger cellular structures and then diluted in filtered PBS (0.1 μm pore size). The samples were then precipitated using Exo-spin Buffer overnight and then centrifuged for 1 hour at 16000g. The obtained pellet with exosomes was resuspended in 100 μL of PBS. Exo-spin columns were prepared with two consecutive washes with 250 μL of PBS at 50 g for 10 sec. Finally, diluted exosomes were passed through the column using 200 μL of PBS and collected in microcentrifuge tubes.

## Nanoparticle Internalization to Exosomes

Suspended exosomes, purified as previously described, were electroporated in 4 mm path length electroporation cuvettes. A single pulse was applied to each exosome sample under the high voltage setting and at an electric field of 0.75 kV/cm. Following electroporation, nanoparticle-loaded exosomes were reisolated using the Exo-spin protocol.

## Characterization of Exosomes

Exosomes were characterized by protein concentration (microBCA assay), shape by scanning transmission electron microscopy (STEM, FEI Quanta 250), concentration and size with NanoSight. The dynamic light scattering system was used to determine the size of exosomes at 25°C in PBS, with a detection angle of 173°. Exosomes were measured at a 1:10 dilution. Western blot analysis was performed to determine the presence of exosome markers EEA1 and TSG101. Cell extracts and exosomes were lysed at 4°C in lysis buffer (50 mm Tris-HCl pH 7.4, 150 mm NaCl, 1 mm EDTA, 1% Triton X-100) supplemented with a cocktail of protease inhibitors [416 μM 4-(2-Aminoethyl)benzenesulfonyl fluoride, 0.32 μM Aprotinin, 16 μM Bestatin, 5.6 μM E-64, 8 μM Leupeptin and 6 μM Pepstatin A; Sigma-Aldrich] and phosphatase inhibitors (1 mm NaF, 0.3 mm $Na_2P_2O_7$ and 1 mm $Na_3VO_4$; Sigma-Aldrich). Cell lysates were collected and lysed for 30 min at 4°C in rotation. Extracts were further centrifuged for 20 min at 13000g at 4°C. Samples with an equivalent amount of protein were denatured at 65°C for 5 min with Laemmli SDS- PAGE sample buffer and analyzed by SDS-PAGE.

## Gold Nanorods Synthesis

For the preparation of a seed solution of gold nanoparticles, a cold-prepared sodium borohydride solution (600 μL, 0.01 M) was added to 250 μL of 0.01 M $HAuCl_4$ in 9.75 mL of 0.1 M cetyltrimethylammonium bromide (CTAB) in a flask, under vigorous magnetic stirring. The seed solution was kept at 27 °C for 2 h, before use. After that, 55 μL of 0.1 M ascorbic acid solution (Sigma Chemical Co., St. Louis, MO, USA) was added to a growth solution containing 75 μL of 0.01 M $AgNO_3$ (Sigma Chemical Co., St. Louis, MO, USA), 9.5 mL of 0.1 M CTAB, and 500 μL of 0.01 M $HAuCl_4$. Further, 250 μL of 0.1 M HCl and 12 μL of the previously prepared seed solution were added. The solution was incubated for 10 min at 27 °C and then centrifuged at a 7030g for 15 min. After centrifugation, the supernatant was removed, and the pellet was resuspended in Milli-Q water.

The GNRs were conjugated with asymmetrical PEGs that have a thiol group (SH) at one end, and a methoxy (HS-PEG-OMe MW 5K, JenKem Technology, TX, USA) or a carboxylic acid group (HS-PEG-COOH MW 5K, JenKem Technology, TX, USA) at the other. A total of 50 μL of 1 mm HS-PEG-OMe in a water solution was added to 10 mL of 1 nM GNRs-CTAB and stirred for 10 min. After centrifugation at RCF of 16100g for 10 min, the pellet was resuspended in 10 mL of Milli-Q water. Subsequently, 300 μL of 1 mm HS-PEG-COOH solution was added into the water solution, and the suspension obtained was stirred for one hour. Further, the suspension was centrifuged at 16100g for 10 min, and the pellet was resuspended in 100 μL of 0.1 M 2-(N- morpholino)ethanesulfonic acid (MES) buffer pH 5.5. Subsequently,

0.2 mg of ethyl-3- (3-dimethylaminopropyl)-carbodiimide (EDC) and 0.5 mg of sulfo-N- hydroxysuccinimide (Sulfo-NHS) in 100 µL of MES were added and mixed for 15 min. The excess of EDC/Sulfo-NHS was subsequently removed by centrifugation at 16100g for 10 min. The resulting pellet was dissolved in phosphate buffered saline (PBS) pH 7.4. The final solution was stirred overnight and centrifuged again the next day, at 16100g for 10 min. Then, the pellet was resuspended in Milli-Q water and stored at 4 °C.

## Characterization of Gold Nanorods and Chinese Ink

The morphology and particle size of SPIONs was investigated by scanning transmission electron microscopy (STEM, FEI Quanta 250) operating at 10.00 kV. The dynamic light scattering system was used to determine the size of nanoparticles at 25°C in Milli-Q water, with a detection angle of 173°. Gold nanorods were measured at a 1:10 dilution, while Chinese ink was measured at a 0.1% dilution. The superficial charge was measured by a Zeta Potential Analyzer. Concentrations obtained from the synthesis were measured using Nanoparticle Tracking Analysis by NanoSight. Chinese ink was obtained from commercially available ARTEL and used at a concentration of 10%.

## Experimental Design for Retrograde and Anterograde Directional Flow Evaluation in Mice

For *post-mortem* anterograde evaluations different nanoparticle solutions (gold nanorods and Chinese ink) were injected into the cisterna magna of C57BL/6 mice (n=3 per condition), after euthanasia by ketamine (300 mg/kg) and xylazine (30 mg/kg) overdose. These were compared with control mice with no injections (n=3). A syringe with a 30G needle was loaded with 50 µL of each solution and administered in the cisterna magna; by placing the mouse in prone position, flexing the head at a 135° angle with the body, and penetrating directly underneath and laterally to the end of the occipital bone towards the foramen magnum through the intact skin. The head and neck were preserved by fixation with 4% paraformaldehyde for histological Gold Enhancement (Nanoprobes GoldEnhance TM LM Kit) analysis.

For *post-mortem* retrograde flow evaluation different nanoparticle solutions (gold nanorods and Chinese ink) were injected into the deep cervical lymph node of C57BL/6 mice (n=3 per condition), after euthanasia by intraperitoneal ketamine (300 mg/kg) and xylazine (30 mg/kg) overdose. These were compared with control mice with no injections (n=3). A syringe with a 30G needle was loaded with 50 µL of each solution and administered into the deep cervical lymph node. To locate the lymph node, skin and subcutaneous tissue were dissected at the midline of the neck, extending the field laterally at the supraclavicular area until both mandibular glands were exposed. Glands were detached from the clavicle surface and moved cranially. The sternocleidomastoid muscles were then displaced until the deep cervical nodes, surrounded by adipose tissue, were identified. The head and neck were preserved by fixation with 4% paraformaldehyde for histological Gold Enhancement (Nanoprobes GoldEnhance TM LM Kit) analysis.

For in vivo anterograde flow evaluation different nanoparticle solutions (SPIONs, exosomes loaded with SPIONs, gold nanorods, and Chinese ink) were injected into the cisterna magna of C57BL/6 mice (n=3 per condition). These were compared with control mice with no injections (n=3). Animals were anesthetized with 5% isoflurane and kept under anesthesia with a nasal cannula supplying 1% isoflurane during the entire procedure. A syringe with a 30G needle was loaded with 10 µL of each solution and administered in the cisterna magna; by placing the mouse in prone position, flexing the head at a 135° angle with the body, and penetrating directly underneath and laterally to the end of the occipital bone towards the foramen magnum through the intact skin. Euthanasia by intraperitoneal sodium thiopental overdose (100 mg/kg) was performed 30 min after injection. The head and neck were preserved by fixation with 4% paraformaldehyde for MRI and histological analysis.

For in vivo retrograde flow evaluation different nanoparticle solutions (SPIONs, exosomes loaded with SPIONs, gold nanorods, and Chinese ink) were injected into the deep cervical lymph node of C57BL/6 mice (n=3 per condition; Chinese ink n=4). These were compared with control mice with no injections (n=3). Animals were anesthetized with 5% isoflurane and kept under anesthesia with a nasal cannula supplying 1% isoflurane during the entire procedure. A syringe with a 30G needle was loaded with 10 µL of each solution and administered into the deep cervical lymph node. To locate the lymph node, skin and subcutaneous tissue were dissected at the midline of the neck, extending the field laterally at the

supraclavicular area until both mandibular glands were exposed. Glands were detached from the clavicle surface and moved cranially. The sternocleidomastoid muscles were then displaced until the deep cervical nodes, surrounded by adipose tissue, were identified. Euthanasia by intraperitoneal sodium thiopental overdose (100 mg/kg) was performed 30 min after injection. The head and neck were preserved by fixation with 4% paraformaldehyde for MRI and histological analysis.

The image acquisition was performed with a clinical Philips Achieva 1.5T MR scanner (Philips Healthcare, Best, Netherlands) and a single-loop surface coil (diameter=47 mm). Perls' Prussian blue was used for iron tissular content analysis. Gold Enhancement (Nanoprobes GoldEnhance TM LM Kit) was used for GNR and Chinese ink analysis.

## Formalin-Fixed, Paraffin-Embedded (FFPE) Tissue Processing for Histology and Special Stains

Whole brain and neck samples were fixed for 24 hours on 4% PFA and then processed for paraffin embedding. Coronal sections of 4 μm were cut from each paraffin block, then sections were dried, deparaffinized and re-hydrated on distilled water. Gold Enhancement was performed with Nanoprobes GoldEnhance TM LM Kit according to manufacturer's instructions. Once this procedure was done, the sections were counterstained with eosin. Nanoparticles were illustrated by Perls' Prussian blue staining for iron content.[13] Tissue was deparaffinized and hydrated with distilled water, immersed in 10% aqueous potassium ferrocyanide and 20% aqueous hydrochloric acid for 20 min. Images of the stained slides were taken with an ICC50W Camera on a DM500 Leica Microscope at 4x, 10x, 20x, and 40x magnification.

Immunohistochemistry analysis was performed on the different sections with joint staining with Gold Enhancement and Perls' Prussian blue to evaluate colocalization with an endothelial marker of lymphatic vessels (LYVE-1). After deparaffinization, antigen recovery was done using buffer Tris-EDTA pH 9.0 in a pressure cooker for 20 min. Endogenous peroxidase was blocked with 3% hydrogen peroxide for 15 min. Blocking of non-specific binding was performed with 3% BSA/PBS for 30 min. Overnight incubation at 4°C with the primary antibody, Recombinant Anti-LYVE1 antibody [EPR21771] (ab218535), was done at 1:5000 dilution. This was followed by incubation with the secondary antibody, Goat Anti-Rabbit IgG H&L (HRP) ab6721 (Abcam), for 1 hour at 25°C. Each slide was then developed with DAB for 1 min. Lung, gall bladder, and spleen tissues were used as controls. Quantification of histological images were performed with the software Image J.

## Animals

All procedures complied with regulations of the Research Ethics Committee of the Pontificia Universidad Católica de Chile. 49 Male C57BL/6 mice were purchased from the animal facility of the Pontificia Universidad Católica de Chile and housed in temperature and humidity-controlled rooms, maintained on a 12h/12h light/dark cycle. Only adult animals (eight to ten weeks) were used in this study. Nine animals were assigned to *post-mortem* anterograde directional flow experiments, nine to *post-mortem* retrograde directional flow analyses, 15 to in vivo anterograde directional flow experiments, and 16 to the in vivo retrograde directional flow group. The sample size was chosen following similar, previously published research.[4,14–16] Animals from different cages in the same experimental group were selected to assure randomization.

## Ethics Approval

All experimental protocols were approved by the Research Ethics Committee of the Pontificia Universidad Católica de Chile, the CEC-CAA (Comité Ético Científico para el Cuidado de Animales y Ambiente), with Protocol ID: 190826005. This study was conducted according to ARRIVE guidelines.

# Results

## MRI Imaging of SPIONs and SPION-Loaded Exosomes in Cervical and Meningeal Lymphatic Vessels

Extracellular vesicles (EVs) are membranous particles naturally emitted by cells, encased in a lipid bilayer, and unable to undergo replication.[17] Exosomes are a subset of EVs that have an endosomal origin and a size range of 40 to 160 nm

(average 100 nm).[18] How EVs can travel between peripheral tissues and the brain in a bidirectional manner remains poorly understood.[10] To investigate if the cervical and meningeal lymphatic network is a possible route for EVs crossing to and from the central nervous system, we prepared exosomes loaded with superparamagnetic iron oxide nanoparticles (SPIONs) to evaluate their anterograde and retrograde directional flow through MRI imaging, leveraging the high efficiency of SPIONs as contrast agents.[19] The anterograde directional flow was defined as the classically described motion of lymphatic components towards the thorax following an injection into the cisterna magna. The retrograde directional flow was defined as nanoparticle motion towards the meningeal lymphatic vessels and the brain after a deep cervical lymph node injection.

We first prepared SPIONs through coprecipitation of ferric and ferrous chlorides with ammonium associated with an acidic pH. This produced SPIONs with mean diameter of 14.28 ± 5.57 nm measured by dynamic light scattering (DLS) (Figure 1a). Scanning transmission electron microscopy (STEM) confirmed SPIONs mean size of 7.08 ± 2.2 nm (Figure 1a). The zeta potential was positive at 36.9 ± 0.51 mV (Figure 1a). After a ten-fold stock dilution with Milli-Q water, pH was increased to 7. Next, we proceeded to isolate exosomes from the B16F10 (ATCC CRL-6475) melanoma cell line using the Exo-spin (CELL GS) protocol. The MicroBCA (ThermoScientific) assay kit was used for total protein quantitation, yielding 300 µg/mL. Western blot analysis confirmed the presence of EV markers EEA1 and TSG101 (Figure 1b). Finally, suspended exosomes were electroporated in 4 mm path length electroporation cuvettes. A single pulse was applied to each exosome sample under the high voltage setting and at an electric field of 0.75 kV/cm. After reisolating the labeled exosomes with Exo-spin columns, DLS revealed an exosome population of an average size of 106 ± 27.35 nm and a mean zeta potential of −17.1 ± 0.53 mV (Figure 1c). Figure 1c shows both B16F10 exosomes and exosomes electroporated with SPIONs as seen by electron microscopy.

To evaluate the retrograde directional flow through the cervical and meningeal lymphatic network, C57BL/6 mice (n=3 per condition) were injected in vivo with a 10 µL solution of either SPIONs (3200 µg/mL) or SPION-loaded exosomes (1.67 x $10^{11}$ particles/mL). These were compared with control mice with no injections (n=3). Animals were anesthetized with 5% isoflurane for 5 min and kept under anesthesia with a nasal cannula supplying 1–2% isoflurane during the entire procedure. A syringe with a 30G needle was loaded with 10 µL of each solution and administered into the deep cervical lymph node. To locate the lymph node, skin and subcutaneous tissue were dissected at the midline of the neck, extending the field laterally at the supraclavicular area until both mandibular glands were exposed. Glands were detached from the clavicle surface and moved cranially. The sternocleidomastoid muscles were then displaced until the deep cervical nodes, surrounded by adipose tissue, were identified. Euthanasia by intraperitoneal sodium thiopental overdose (100 mg/kg) was performed 30 min after injection. The head and neck were preserved by fixation with 4% paraformaldehyde for MR imaging (Philips Achieva 1.5 T MR scanner) and histological analysis.

Both SPIONs and SPION-loaded exosomes revealed hypointense signals in the brain ventricles and parenchyma, particularly in the T2* MRI maps (Figure 2a). Hypointense signals were also detected at the level of the neck where the injections were administered. Retrograde directional flow of SPIONs injected into the deep cervical lymph node in vivo was observed in staining of neck and head lymphatic vessels, including meningeal lymphatics, in all mice (n=3) (Supplementary Figures S1 and S2c). However, no staining was observed within the brain parenchyma with the Perls' Prussian Blue technique. Iron detection through this staining method is prone to yield false negatives, as the detection requires the accumulation of several hundreds of nm in diameter,[20] which could hinder signals from SPIONs smaller than 10 nm diluted in the volume of the brain parenchyma. Combined Perls' Prussian Blue staining and anti-LYVE-1 (lymphatic vessel endothelial hyaluronan receptor-1) immunohistochemistry revealed nanoparticles within the cervical lymphatic vessels towards the meningeal lymphatic vessels in the in vivo retrograde directional flow experiments performed on all C57BL/6 mice (n=3). No SPION staining was detected within arterial or venous structures within the head and neck (Supplementary Figure S3b). As expected, exosomes loaded with SPIONs did not stain, indicating the presence of iron nanoparticles within exosome membranes.

To evaluate the anterograde directional flow, we injected C57BL/6 mice (n=3 per condition) in vivo with a 10 µL solution of either SPIONs (3200 µg/mL) or SPION-loaded exosomes (1.67 x 1011 particles/mL). These were compared with control mice with no injections. Animals were anesthetized with 5% isoflurane and kept under anesthesia with a nasal cannula supplying 1% isoflurane during the entire procedure. A syringe with a 30G needle was loaded with 10 µL

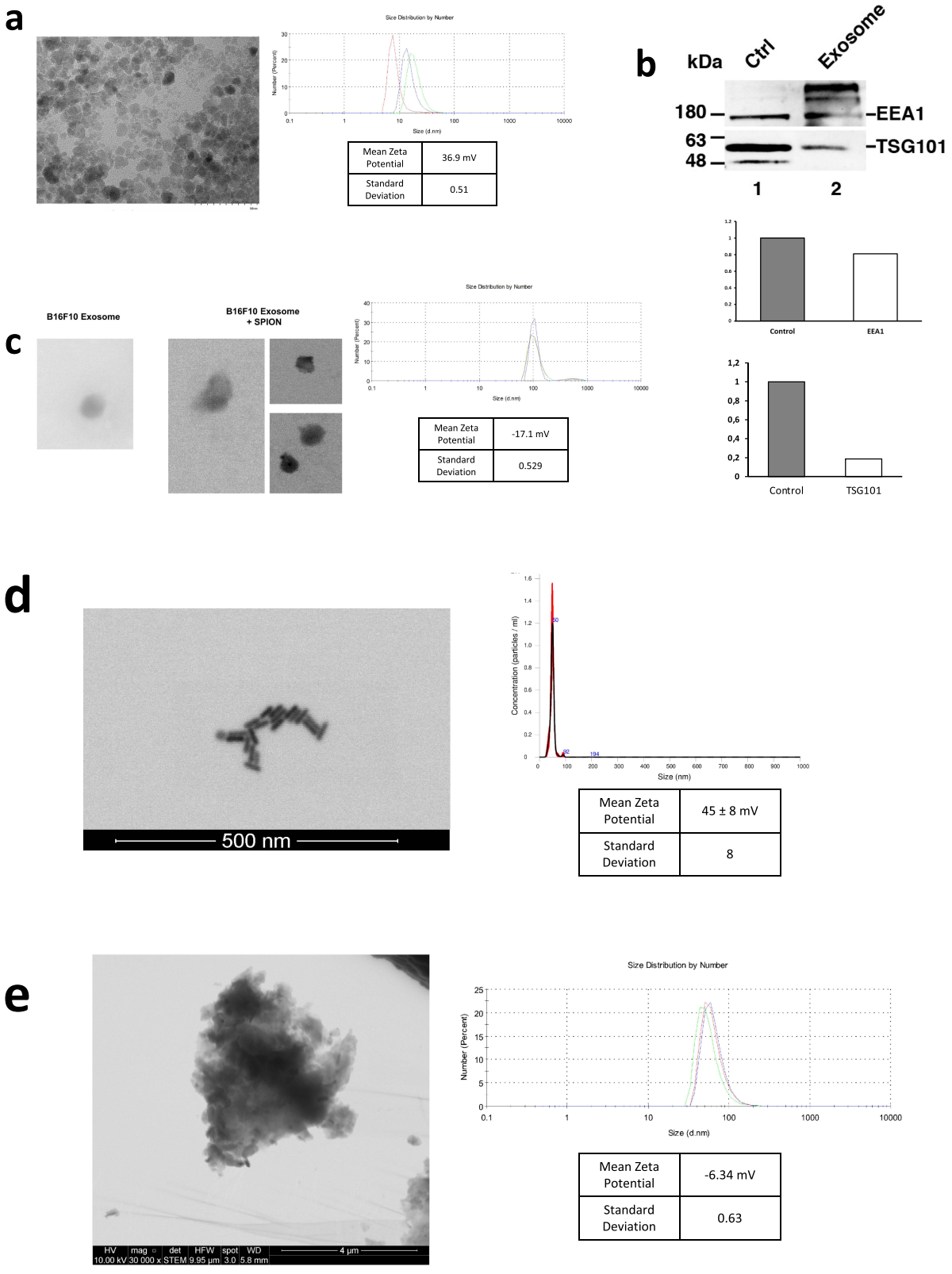


**Figure 1** Characterization of nanoparticles. (**a**) STEM visualization of SPIONs; size distribution and zeta potential measured by DLS. (**b**) Western blot of EV markers EEA1 and TSG101 on exosomes from the B16F10 melanoma cell line. Control was performed using a cellular extract from the B16F10 cell line. Quantification of EEA1 and TSG101 with respect to control is shown. (**c**) STEM visualization of exosomes with and without SPIONs labeling; size distribution and zeta potential measured by DLS. (**d**) STEM visualization of gold nanorods; size distribution measured by NTA and zeta potential determined by DLS. (**e**) STEM visualization of Chinese ink; size distribution and zeta potential measured by DLS.

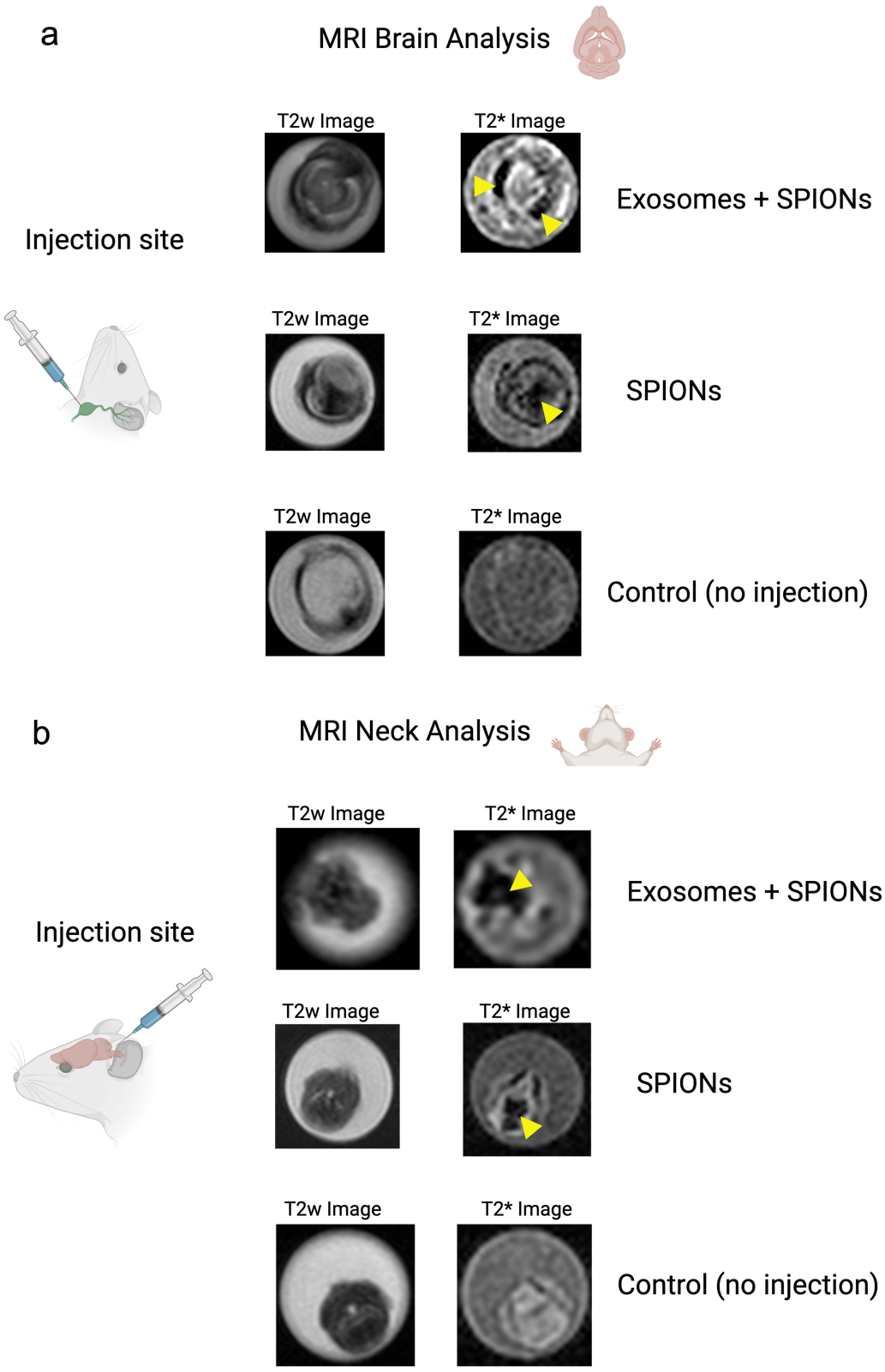


**Figure 2** Directional flow analysis by MRI of SPIONs and SPION-labeled exosomes through the cervical and meningeal lymphatic network. (**a**) Retrograde Directional Analysis: Brain images reveal the detection of nanoparticles in this region 30 minutes after injection into the deep cervical lymph node (n=3), particularly evident in the T2* map (yellow arrows). These two conditions were compared to control mice with no injected solutions (n=3). (**b**) Anterograde Directional Analysis: Neck images reveal the detection of nanoparticles in this region 30 minutes after injection into the cisterna magna (n=3), particularly evident in the T2* map (yellow arrows). These two conditions were compared to control mice with no injected solutions (n=3).

of each solution and administered into the cisterna magna; by placing the mouse in prone position, flexing the head at a 135° angle with the body, and penetrating directly underneath and laterally to the end of the occipital bone towards the foramen magnum through the intact skin. Euthanasia by intraperitoneal sodium thiopental overdose (100 mg/kg) was performed 30 min after injection. The head and neck were preserved by fixation with 4% paraformaldehyde for 1.5 Tesla MRI scanner and histological analysis.

Both SPIONs and SPION-loaded exosomes showed hypointense signals of cervical lymphatic structures after intracerebroventricular injections through the cisterna magna, as seen in the T2w images and T2* maps (Figure 2b). Anterograde directional flow in in vivo procedures (n=3) of SPIONs after administration into the cisterna magna was confirmed by the detection of Perls' Prussian Blue staining in cervical lymphatic vessels in all mice (Supplementary Figure S4). At the level of the head, the injection into the cisterna magna also showed staining within the ventricles. As expected, exosomes loaded with SPIONs did not stain, indicating the presence of iron nanoparticles within exosome membranes.

Together, MRI imaging results indicate that the cervical and meningeal lymphatic network can transport SPIONs and SPION-labeled exosomes both towards the thorax and in the direction of the brain.

## Gold Nanorods Bidirectional Motion Through the Cervical and Meningeal Lymphatic Network

With MRI imaging suggesting the possibility of retrograde flow of SPIONs and SPION-loaded exosomes towards the brain after a cervical administration, we further examined other nanoparticles that could be more effectively assessed through histological techniques in the brain parenchyma. This also allowed the evaluation of different alternatives that can be subsequently explored in pharmacology and nanomedicine. Therefore, we used gold nanorods functionalized with polyethylene glycol (GNR-PEG) as described in Methods. GNR-PEG with a mean size of 49.1 ± 0.9 nm and mean zeta potential of 45 ± 8 mV were obtained and measured by DLS and Nanoparticle Tracking Analysis (NTA) (Figure 1d). GNR-PEG morphology can be observed in the STEM image seen in Figure 1d. The GNR-PEG size distribution determined by STEM showed a length of 34.6 ± 4.2 nm and a width of 11.4 ± 1.6 nm. The anterograde and retrograde directional flow were evaluated in two scenarios with *post-mortem* or in vivo administrations of GNR-PEG solutions in C57BL/6 mice (n=3 per condition) into the cisterna magna or the deep cervical lymph node. These interventions were compared with control mice with no injections (n=3).

*Post-mortem* procedures were performed using 50 µL of GNR-PEG at a concentration of $1.71\times10^{14}$ particles/mL. Dissections for identifying the deep cervical lymph node during retrograde administrations followed the method described previously for in vivo procedures. The head and neck were preserved by fixation with 4% paraformaldehyde for histological Gold Enhancement (Nanoprobes GoldEnhance TM LM Kit) analysis. Retrograde directional flow in *post-mortem* procedures (n=3) of gold nanorods after deep cervical lymph node administration was confirmed by the detection of Gold Enhancement staining at different CNS regions in all mice. These included the olfactory bulb, the brain parenchyma, and within the meningeal lymphatic vessels (Figure 3a). No staining was detected within arterial or venous structures within the head and neck, ruling out other sources of nanoparticle distribution to the brain in *post- mortem* GNR-PEG assays. Control mice with no GNR-PEG administrations showed no Gold Enhancement staining in any anatomical structure.

Anterograde directional flow in *post-mortem* procedures (n=3) of GNR-PEG after administration into the cisterna magna was also confirmed by the detection of Gold Enhancement staining in cervical lymphatic vessels in all mice, as well as in the connective tissue of the neck (Figure 4a). Gold nanoparticles were also identified in the cervical spinal cord as well as its surrounding subdural space and associated peripheral nerves (Figure 4a). At the level of the head, the injection into the cisterna magna also showed staining within lateral ventricles, the third ventricle, the olfactory bulb, and the optic chiasm in all mice. No Gold Enhancement staining was observed in any anatomical structure of the control mice that did not receive GNR-PEG administrations.

To investigate the directional flow of GNR-PEG under physiological conditions and to minimize the potential impact of volume, we administered 10 µL of GNR-PEG at a concentration of $1.71\times10^{14}$ particles/mL in vivo. The administration technique was as previously described for deep cervical lymph node and cisterna magna injections. Combined Gold Enhancement and anti-LYVE-1 immunohistochemistry revealed gold nanoparticles within the cervical and meningeal lymphatic vessels in the in vivo retrograde directional flow experiments performed on all C57BL/6 mice (n=3)

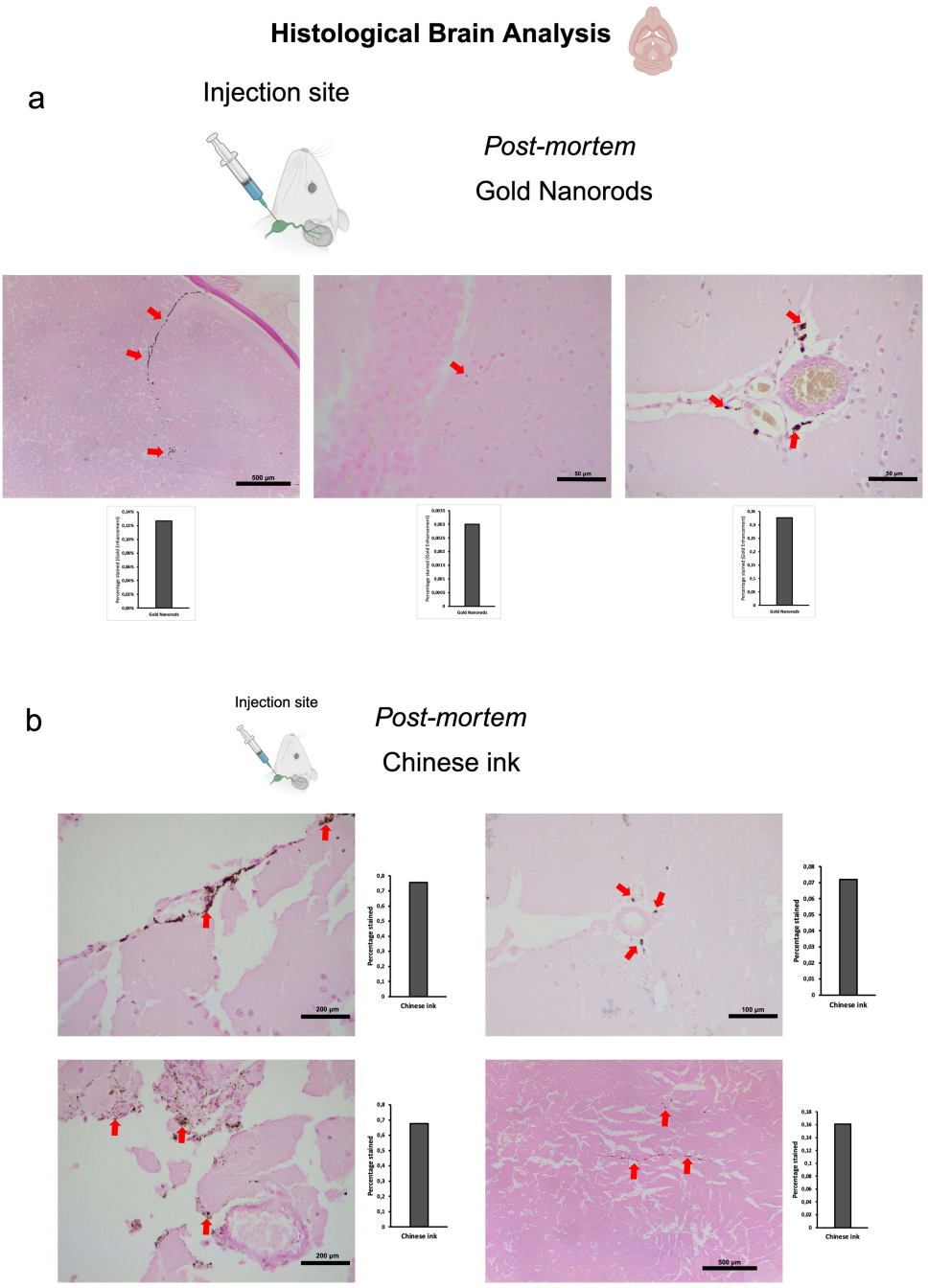


**Figure 3** Retrograde directional flow analysis by brain histology after *post-mortem* nanoparticle administration into the deep cervical lymph node. (**a**) Gold nanorods were identified by the Gold Enhancement technique in the olfactory bulb, the brain parenchyma, and the meningeal lymphatic vessels (red arrows) (n=3). (**b**) Chinese ink nanoparticles stained the meningeal lymphatic vessels, the brain parenchyma, and the third ventricle wall (red arrows) (n=3).

(Figure 5a). GNR-PEG also reached the brain parenchyma through the retrograde flow from the cervical lymphatic vessels in all mice (Figure 5a). GNR-PEG were found staining within anti-LYVE1 cervical lymphatic vessels towards the meningeal lymphatics (Supplementary Figure S2a). No staining was detected within arterial or venous structures within the head and neck, ruling out other sources of nanoparticle distribution to the brain in in vivo gold nanoparticle assays (Supplementary Figure S3a). Anterograde directional flow of gold nanoparticles after administration into the cisterna magna in vivo was established by the detection of Gold Enhancement staining in cervical lymphatic vessels in all mice (Figure 6a). Gold Enhancement staining was not detected in any anatomical structure of the control mice that did not undergo GNR-PEG administrations.

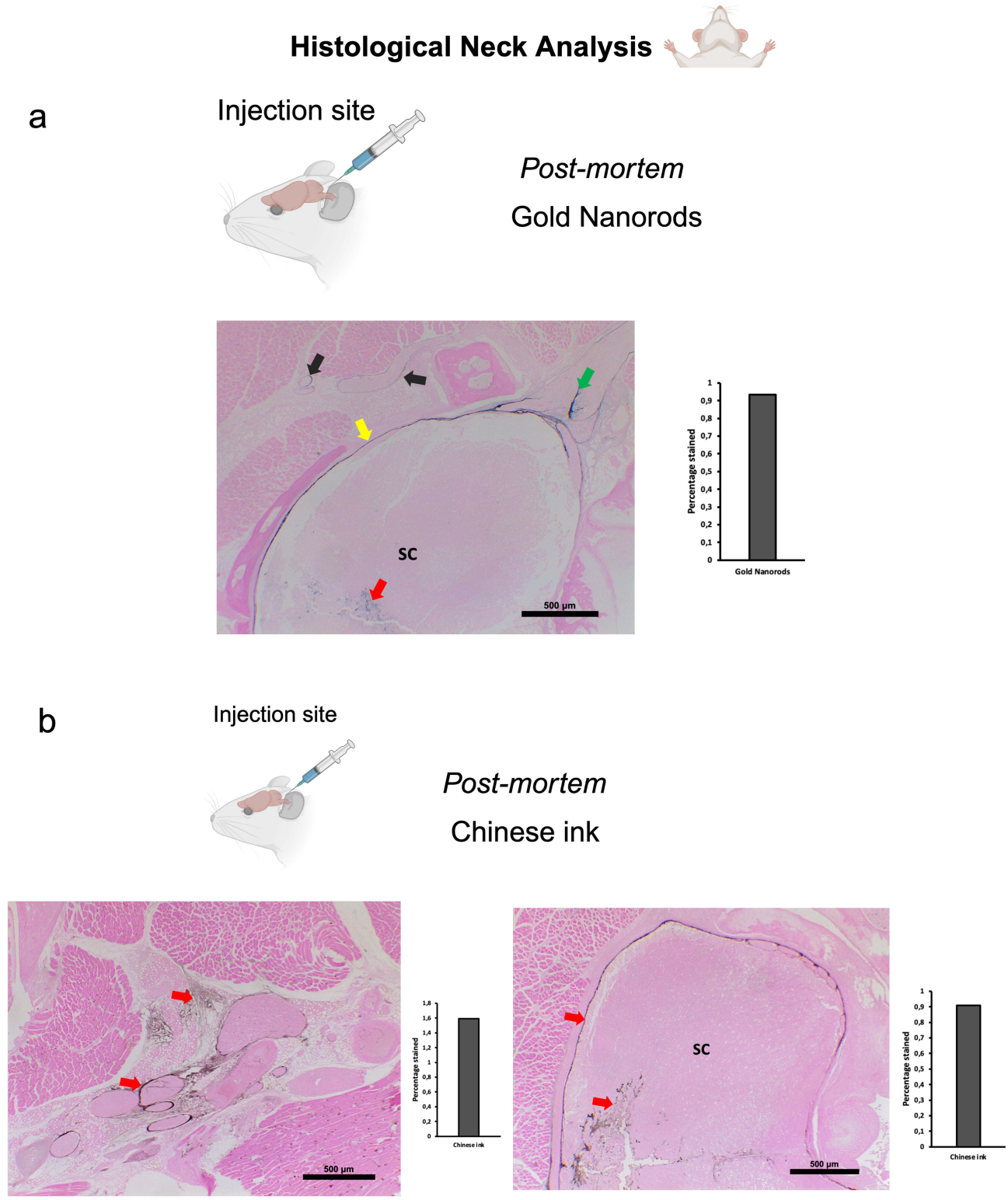


**Figure 4** Anterograde directional flow analysis by brain histology after *post-mortem* nanoparticle administration into the cisterna magna. (**a**) Gold Enhancement showed staining of the cervical spinal cord (red arrow), its surrounding subdural space (yellow arrow) and associated peripheral nerves (green arrow). Gold nanoparticles were also detected in cervical lymphatic vessels and connective tissue (black arrows) (n=3). (**b**) Chinese ink nanoparticles were identified in cervical lymphatic vessels, connective tissue, as well as the cervical spinal cord and its surrounding subdural space (indicated by red arrows) (n=3).
**Abbreviation**: SC, spinal cord.

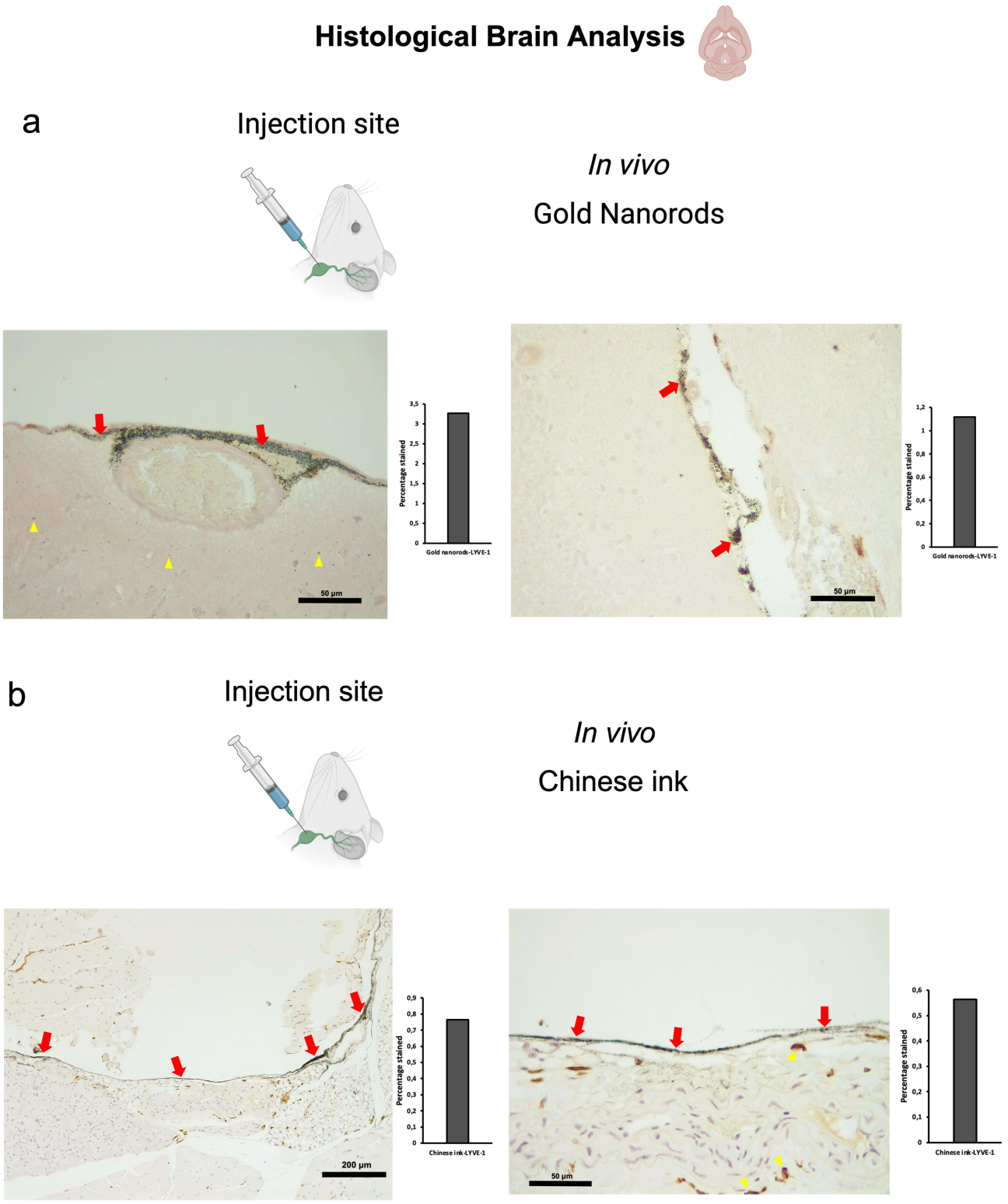


**Figure 5** Retrograde directional flow analysis by brain histology after in vivo nanoparticle administration into the deep cervical lymph node. (**a**) Combined Gold Enhancement and anti-LYVE-1 immunohistochemistry showed gold nanorods within meningeal lymphatic vessels (red arrows) and the brain parenchyma (yellow arrows), with no staining within cerebral arteries (n=3). (**b**) Meningeal lymphatic vessels stained with anti-LYVE-1 immunohistochemistry and colocalized with Chinese ink nanoparticles (red arrows). Chinese ink was also identified in the brain parenchyma (yellow arrows) (n=4).
**Abbreviation**: LYVE-1, lymphatic vessel endothelial hyaluronan receptor-1.

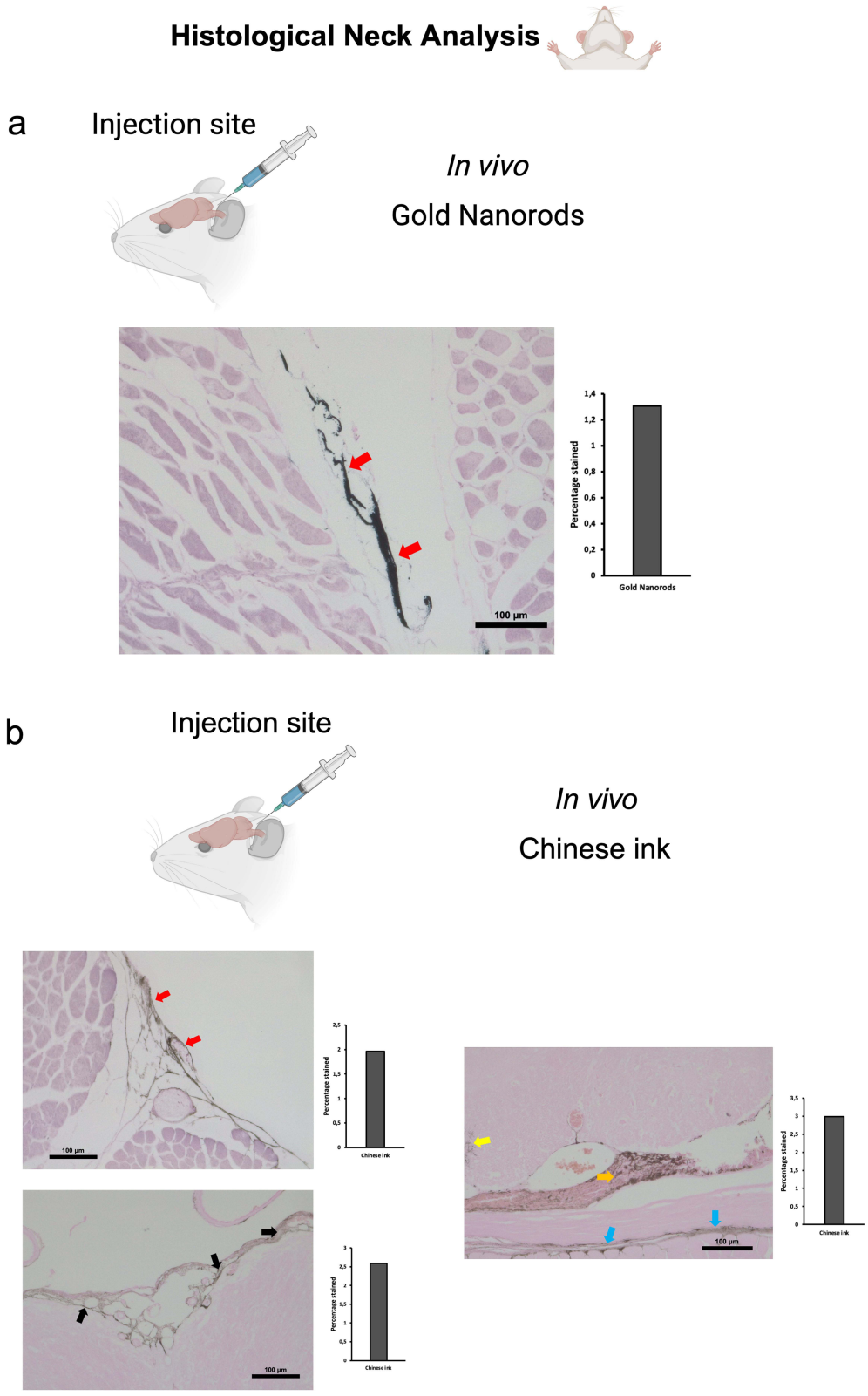


**Figure 6** Anterograde directional flow analysis by brain histology after in vivo nanoparticle administration into the cisterna magna. (**a**) Gold Enhancement showed staining of lymphatic vessels in the cervical region (red arrows) (n=3). (**b**) Chinese ink nanoparticles were identified in the cervical lymphatic vessels (red arrows), the subarachnoid space (black arrows), as well as the cervical spinal cord (yellow arrow), peripheral nerves (Orange arrow), and connective tissue (blue arrows) (n=3).

The results of histological analyses collectively suggest that the cervical and meningeal lymphatic network is capable of bidirectional transportation of gold nanorods, encompassing movement towards both the thorax and the brain.

## Chinese Ink Bidirectional Motion Through the Cervical and Meningeal Lymphatic Network

Chinese ink has been previously used for staining of lymphatic structures,[21–23] which led to its consideration for our evaluation on the bidirectional motion of nanoparticles through the cervical and meningeal lymphatic network. Interestingly, Chinese ink (Artel, Santiago, Chile) was characterized by DLS, which revealed nanoparticles with a mean (± SD) size of 61.62 ± 4.84 nm and mean (± SD) surface zeta potential of −6.34 ± 0.63 mV (Figure 1e), which are measurements similar to the range values observed in purified exosomes. To our surprise, we found that Chinese ink can also be stained with the Gold Enhancement technique (Nanoprobes GoldEnhance TM LM Kit) used previously with GNR, confirmed by the lack of staining of control mice brain parenchyma slides with no nanoparticle administration. The anterograde and retrograde directional flow were evaluated after *post-mortem* and in vivo administrations of Chinese ink solutions in C57BL/6 mice (n=3 per condition) in the cisterna magna and the deep cervical lymph node, respectively. These were compared with control mice with no injections (n=3).

*Post-mortem* procedures were performed using 50 µL of 10% Chinese ink (Artel, Santiago, Chile). Dissections for identifying the deep cervical lymph node during retrograde administrations followed the method described previously for procedures with SPION-loaded exosomes. The head and neck were preserved by fixation with 4% paraformaldehyde for histological Gold Enhancement (Nanoprobes GoldEnhance TM LM Kit) analysis. Retrograde directional flow in *post-mortem* procedures (n=3) of Chinese ink after deep cervical lymph node administration was confirmed by the detection of Gold Enhancement staining at different CNS regions in all mice (Figure 3b). Staining was detected within the meningeal lymphatic vessels, the third ventricle, and cortical regions near meningeal lymphatic vessels. No staining was detected within arterial or venous structures within the head and neck, ruling out other sources of nanoparticle distribution to the brain in *post-mortem* Chinese ink assays. In control mice that did not undergo Chinese ink administrations, there was no presence of Gold Enhancement staining in any anatomical structure.

Anterograde directional flow in post-mortem procedures (n=3) of Chinese ink nanoparticles after administration into the cisterna magna was confirmed by the detection of staining in cervical lymphatic vessels in all mice, as well as in connective tissue of the neck (Figure 4b). Chinese ink nanoparticles were also identified in the cervical spinal cord as well as its surrounding subdural space (Figure 4b). At the level of the head, the injection into the cisterna magna also showed staining within lateral ventricles. The anatomical structures of the control mice that did not receive Chinese ink administrations exhibited no signs of Gold Enhancement staining.

To examine the Chinese ink directional flow under physiological conditions and reducing the potential effects of volume, we conducted in vivo administrations of 10 µL of 10% Chinese ink (Artel, Santiago de Chile). The administration procedure followed the previously established method for injections into the deep cervical lymph nodes and the cisterna magna. Retrograde directional flow of in vivo procedures (n=4) was confirmed in all mice after deep cervical lymph node administration. Combined Gold Enhancement and anti-LYVE-1 immunohistochemistry showed Chinese ink within the meningeal lymphatic vessels and cortical regions near these lymphatic structures (Figure 5b). One mouse died at minute two before the expected completion time of 30 min before euthanasia. Nevertheless, after histological analysis of this specimen, Chinese ink nanoparticles were identified in the meningeal lymphatic vessels and the brain parenchyma. Chinese ink was found staining within anti-LYVE1 cervical lymphatic vessels towards the meningeal lymphatics (Supplementary Figure S2b). No staining was detected within arterial or venous structures within the head and neck of two out of three mice (Supplementary Figure S3c). One mouse presented staining within the jugular vein but not the carotid artery (Supplementary Figure S3), which also indicates that the observed nanoparticles at the meningeal lymphatic vessels and the brain parenchyma originate mainly from the lymphatic system distribution and not through arterial circulation of cardiac and other thoracic vessels. Anterograde directional flow in in vivo procedures (n=3) after administration into the cisterna magna was confirmed by the detection of staining in cervical lymphatic vessels in all mice (Figure 6b). Chinese ink nanoparticles were also identified in the subarachnoid space, the cervical spinal cord, and

peripheral nerves (Figure 6b). No staining was observed in any anatomical structure of the control mice that did not receive any administrations.

Taken together, the findings of histological analyses indicate that the cervical and meningeal lymphatic network is capable of bidirectional transportation of Chinese ink nanoparticles, involving movement towards both the thorax and the brain.

## Discussion

We have shown evidence that suggests that the cervical and meningeal lymphatic network can transport nanoparticles not only in the classically described lymphatic drainage towards the thorax but can also serve as an access gate to the brain. SPIONs and SPION-loaded exosomes were detected by MRI in the brain of C57BL/6 mice after deep cervical lymph node administration in vivo. Gold nanorods and Chinese ink nanoparticles were also identified within the meningeal lymphatic vessels and the brain parenchyma of mice in the retrograde directional flow histological analysis from cervical injections in *post-mortem* and in vivo procedures. Anterograde directional flow experiments from all nanoparticle experiments also showed motion from the cisterna magna to the deep cervical lymph nodes. Together, these indicate that the system allows for bidirectional flow after administration.

Two pertinent factors to examine regarding the described retrograde lymphatic flow towards the brain include alternative vascular pathways and the influence of pressure exerted at the cervical injection site. The initial consideration, particularly in in vivo assays, was whether nanoparticles in meningeal lymphatic vessels and the brain might have originated from their distribution from the cervical lymphatic vessels, passing through the jugular vein, the superior vena cava, the right atrium and ventricle of the heart, through the pulmonary circulation, to the left atrium and ventricle of the heart, and towards the carotid arteries before entering the cerebral circulation. This would entail that nanoparticles would have been present in histological analyses within the jugular veins and the common carotid arteries during cervical examinations. However, as previously indicated, all in vivo SPION, GNR-PEG, and Chinese ink retrograde experiments (collectively n=10) showed no staining of carotid arteries. Moreover, nine out of the ten deep cervical lymphatic nanoparticle administrations showed no staining of jugular veins. GNR-PEG and Chinese ink post-mortem retrograde injections (collectively n=6) also concurred with these findings. Given that nanoparticles were indeed found staining within anti-LYVE1 cervical lymphatic vessels towards the meningeal lymphatics, this data supports the conclusion that nanoparticles reaching the brain were following a lymphatic pathway.

It is important to consider that although the volume injected in in vivo procedures was small (10 μL) the pressure exerted at the cervical injection site could have been significantly greater than the intranodal pressure, changing the fluid dynamics within the lymph node. However, this relationship is complex to determine at this stage because cervical intranodal pressures have not yet been established. Previous studies have analyzed intranodal pressure of other anatomical locations in mice with different results. Bouta et al described intranodal popliteal and axillary pressures of an average 9 and 12 cm$H_2O$, respectively, in normal wild type mice.[24] Kato et al and Miura et al used MXH10/Mo-lpr/lpr, a mouse model that develops systemic swelling of lymph nodes, obtaining lower values for intranodal pressures.[25,26] Miura et al showed that mean pressures within subiliac and axillary nodes were 0.10 cm $H_2O$ and 0.03 cm $H_2O$, respectively.[26] When examining their data, Kato et al found subiliac lymph nodes with a mean pressure of 1.63 cm $H_2O$.[25] Finally, Rohner et al have even described subatmospheric pressures of −1 cm $H_2O$ in axillary and brachial lymph nodes of immune-competent C57Bl/6 mice.[27]

Another factor to consider is that the pressure that can be produced for any syringe at a predetermined speed depends on the force applied divided by the surface area of the syringe plunger.[28] While humans can apply considerable forces to a plunger, with an average maximum force of 79N, this implies that a lower injection force is needed to generate equivalent pressures when syringe caliber is reduced.[28] Therefore, injections performed by a human operator may differ considerably in force and pressure exerted depending on the syringe caliber and intranodal state. Future research should address cervical intranodal pressures and the biomechanics of fluid administration to better understand the fluid dynamics of this anatomical region.

It should be highlighted that mice and human functional anatomy of dural lymphatics has been found to be conserved. Jacob et al found similar circa-cerebral meningeal lymphatic architecture and relationship with dural venous sinuses, with

limited connections with the nasal lymphatic bed, and a conserved pattern of cavernous sinus associated vessels penetrating the skull through several bilateral foramina of the skull base.[29] They emphasized that murine models are relevant to predict the pathophysiological contribution of the dural lymphatic system and test lymphatic-targeted drugs in neurological disease models.[29] Here we evaluated different nanoparticles with pharmacological applications through these lymphatic vessels and point to a bidirectional potential that opens the possibility of an alternative access to the brain. Our experiments therefore can also give insights into possible human fluid dynamics that should be explored.

The exact drivers of this bidirectional flow could involve pressure changes within the lymphatic vessels and nodes in a system with few valves and no smooth muscle cell lining when entering the head. This means that anatomical position changes or physiological changes in pressure surrounding lymphatic tissues could create conditions favoring motion in the retrograde or anterograde flow when necessary. Pathological conditions producing pressure changes in or around lymphatic tissues could also promote and determine directional flow in the cervical and meningeal lymphatic network. Particularly in mammals such as humans that experience radical changes in head and neck dynamics with the upright and recumbent position, the possibility of bidirectional lymphatic flow could be relevant in many physiological processes such as during sleep. Interestingly, nanoparticles reached the meningeal lymphatic vessels and the brain parenchyma independently of superficial charge. SPIONs (36.9 ± 0.51 mV) and GNR-PEG (45 ± 8 mV) were positively charged, while exosomes (−17.1 ± 0.53 mV) were negatively charged. Chinese ink nanoparticles (−6.34 ± 0.63 mV) exhibited a more neutralized negative charge. Although previous reports suggest that nanoparticles with either negative or positive surface charges facilitate lymph node accumulation,[7] Mc.Cright et al demonstrated that neutral nanoparticles enhance delivery to lymphatic vessels by modulating the cell transport mechanism.[30] Therefore, surface charge should be carefully considered in future applications of nanoparticle transport through the cervical and meningeal lymphatic network.

The pharmacological implications of our findings could be important in the field of nanomedicine. The methodology used for labeling exosomes in this project could be modified to carry drugs through the lymphatic system and improve specific distribution to the brain. Further studies can evaluate if an interstitial injection in the neck could deliver enough nanoparticles through this system to develop noninvasive treatment procedures, as homing characteristics to lymph nodes have been seen in previous studies of SPION-loaded exosomes to popliteal lymphatics.[15] Given that cancer exosomes could potentially move towards the brain through this pathway, and that an anecdotal case report has suggested that cancer cells can move in a retrograde lymphatic manner in other organs even in valve-equipped lymphatic vessels,[31] mortality in these patients would be substantially reduced if cerebral metastatic mechanisms could be prevented. In this regard, future investigations can delve into cancer exosome lymphatic inhibitors, by regulating or blocking movement through these vessels.

In neurodegenerative diseases, the use of promising peptide inhibitors of polyglutamine aggregation (QBP1, NT17, and PGQ9P2) in Huntington's disease has been hindered precisely because of poor BBB penetration and low bioavailability.[32] A cervical lymphatic route could be an attractive pathway to evaluate more efficient means for accessing the brain without complex nanoparticle constructions. A recent publication by Dominy et al has associated *P. gingivalis* with Alzheimer's disease.[33] Bacterial DNA and RNA found in the brain of patients with this disease could be transported by exosomes through the lymphatic system. Other rapidly rising fields, such as the connection between the gut microbiota with diseases such as autism, neurological disorders like multiple sclerosis, and mental disorders,[34] could potentially involve retrograde lymphatic flow of exosomes and different nanoparticles towards the brain.

## Conclusion

In conclusion, the cervical and meningeal lymphatic network can serve as an access route for nanoparticles to the brain, allowing bidirectional flow. This mechanism of the meningeal lymphatic pathway could be exploited in the theranostic field of nanomedicine to deliver drugs for the treatment of various neurological diseases. Additionally, our findings using exosomes from the metastatic B16F10 melanoma cell line could aid in a more profound comprehension of brain metastasis pathophysiology regarding the participation of extracellular vesicles.

## Abbreviations

BBB, Blood–brain barrier; CEC-CAA, Comité Ético Científico para el Cuidado de Animales y Ambiente; CNS, central nervous system; CTAB, cetyltrimethylammonium bromide; DLS, dynamic light scattering; EDC, ethyl-3- (3-dimethylaminopropyl)-carbodiimide; EEA1, early endosome antigen 1; EVs, extracellular vesicles; GNRs, gold nanorods; GNR-PEG, gold nanorods functionalized with polyethylene glycol; ICP MS, inductively coupled plasma mass spectrometry; LYVE-1, endothelial marker of lymphatic vessels; MES, 2-(N- morpholino)ethanesulfonic acid; MRI, magnetic resonance imaging; NTA, nanoparticle tracking analysis; PBS, phosphate buffered saline; PEG, polyethylene glycol; SD, standard deviation; SPIONs, superparamagnetic iron oxide nanoparticles; STEM, scanning transmission electron microscopy; TSG101, tumor susceptibility gene 101.

## Data Sharing Statement

The data that support the findings of this study are available from the corresponding author upon reasonable request.

## Ethics Approval

All experimental protocols were approved by the Research Ethics Committee of the Pontificia Universidad Católica de Chile, the CEC-CAA (Comité Ético Científico para el Cuidado de Animales y Ambiente), with Protocol ID: 190826005. This study was conducted according to ARRIVE guidelines.

## Acknowledgments

We thank Sergio Alvarez for his collaboration with electroporation equipment. The authors acknowledge Wilda Olivares, Andrés Rodriguez, Pablo Santoro, Ignacio Wichmann, Rocío Bustos, Leticia Gonzalez, Miguel Urrutia, Mauricio Cuello, and Flavia Zacconi for comments and assistance. This study was supported by ANID BECAS/DOCTORADO NACIONAL 21211334; ANID - Millennium Science Initiative Program - ICN2021_004, ANID – FONDECYTs 1220922, 1231773 and 1211482; CONICYT-FONDAP 15130011, FONDAP 1523A0008A, FONDEQUIP NTA (EQM160157), and FONDEQUIP SEM (EQM170111). This paper has been uploaded to biorxiv as a preprint: https://www.biorxiv.org/content/10.1101/2024.01.06.574478v1.full

## Author Contributions

All authors made a significant contribution to the work reported, whether that is in the conception, study design, execution, acquisition of data, analysis and interpretation, or in all these areas; took part in drafting, revising or critically reviewing the article; gave final approval of the version to be published; have agreed on the journal to which the article has been submitted; and agree to be accountable for all aspects of the work.

## Funding

This study was supported by ANID BECAS/DOCTORADO NACIONAL 21211334; ANID - Millennium Science Initiative Program - ICN2021_004, ANID – FONDECYTs 1220922, 1231773 and 1211482; CONICYT-FONDAP 15130011, FONDAP 1523A0008A, FONDEQUIP NTA (EQM160157), and FONDEQUIP SEM (EQM170111).

## Disclosure

The authors declare no competing interests in this work.

## References

1. Hershenhouse KS, Shauly O, Gould DJ, Patel KM. Meningeal lymphatics: a review and future directions from a clinical perspective. *neuroscience Insights*. 2019;14:1179069519889027. doi:10.1177/1179069519889027
2. Jiang H, Wei H, Zhou Y, Xiao X, Zhou C, Ji X. Overview of the meningeal lymphatic vessels in aging and central nervous system disorders. *Cell Biosci*. 2022;12(1):202. doi:10.1186/s13578-022-00942-z
3. Ali Khan A, Mudassir J, Mohtar N, Darwis Y. Advanced drug delivery to the lymphatic system: lipid-based nanoformulations. *Int J Nanomed*. 2013;8:2733–2744. doi:10.2147/IJN.S41521

4. Louveau A, Smirnov I, Keyes TJ, et al. Structural and functional features of central nervous system lymphatic vessels. *Nature*. 2015;523 (7560):337–341. doi:10.1038/nature14432
5. Aspelund A, Antila S, Proulx ST, et al. A dural lymphatic vascular system that drains brain interstitial fluid and macromolecules. *J Exp Med*. 2015;212(7):991–999. doi:10.1084/jem.20142290
6. Qi S, Wang X, Chang K, Shen W, Yu G, Du J. The bright future of nanotechnology in lymphatic system imaging and imaging-guided surgery. *J Nanobiotechnology*. 2022;20(1):24. doi:10.1186/s12951-021-01232-5
7. Lee J, Kang S, Park H, Sun JG, Kim EC, Shim G. Nanoparticles for lymph node-directed delivery. *Pharmaceutics*. 2023;15(2). doi:10.3390/pharmaceutics15020565
8. Hardesty DA, Nakaji P. The current and future treatment of brain metastases. *Front Surg*. 2016;3:30. doi:10.3389/fsurg.2016.00030
9. Geetha R, Janardhanan M, Thankappan KK. Premetastatic niche: a novel area for research in metastasis with a potential as therapeutic targeting in oral cancer. *J Pharm Bioallied Sci*. 2023;15(Suppl 1):S36–S39. doi:10.4103/jpbs.jpbs_49_23
10. Ramos-Zaldívar HM, Polakovicova I, Salas-Huenuleo E, et al. Extracellular vesicles through the blood-brain barrier: a review. *Fluids Barriers CNS*. 2022;19(1):60. doi:10.1186/s12987-022-00359-3
11. Xu JQ, Liu QQ, Huang SY, et al. The lymphatic system: a therapeutic target for central nervous system disorders. *Neural Regen Res*. 2023;18 (6):1249–1256. doi:10.4103/1673-5374.355741
12. Liblau RS, Gonzalez-Dunia D, Wiendl H, Zipp F. Neurons as targets for T cells in the nervous system. *Trends Neurosci*. 2013;36(6):315–324. doi:10.1016/j.tins.2013.01.008
13. Grauer O, Jaber M, Hess K, et al. Combined intracavitary thermotherapy with iron oxide nanoparticles and radiotherapy as local treatment modality in recurrent glioblastoma patients. *J Neurooncol*. 2019;141(1):83–94. doi:10.1007/s11060-018-03005-x
14. Da Mesquita S, Louveau A, Vaccari A, et al. Functional aspects of meningeal lymphatics in ageing and Alzheimer's disease. *Nature*. 2018;560:7717):185–191. doi:10.1038/s41586-018-0368-8
15. Hu L, Wickline SA, Hood JL. Magnetic resonance imaging of melanoma exosomes in lymph nodes. *Magn Reson Med*. 2015;74(1):266–271. doi:10.1002/mrm.25376
16. Ahn JH, Cho H, Kim JH, et al. Meningeal lymphatic vessels at the skull base drain cerebrospinal fluid. *Nature*. 2019;572(7767):62–66. doi:10.1038/s41586-019-1419-5
17. Théry C, Witwer KW, Aikawa E, et al. Minimal information for studies of extracellular vesicles 2018 (MISEV2018): a position statement of the International Society for Extracellular Vesicles and update of the MISEV2014 guidelines. *J Extracell Vesicles*. 2018;7(1). doi:10.1080/20013078.2018.1535750
18. Kalluri R, LeBleu VS. The biology, function, and biomedical applications of exosomes. *Science*. 2020;367(6478). doi:10.1126/science.aau6977
19. Vangijzegem T, Lecomte V, Ternad I, et al. Superparamagnetic Iron Oxide Nanoparticles (SPION): from fundamentals to state-of-the-art innovative applications for cancer therapy. *Pharmaceutics*. 2023;15(1). doi:10.3390/pharmaceutics15010236
20. Curdt F, Haase K, Ziegenbalg L, Greb H, Heyers D, Winklhofer M. Prussian blue technique is prone to yield false negative results in magnetoreception research. *Sci Rep*. 2022;12(1):8803. doi:10.1038/s41598-022-12398-9
21. Q CAO, WANG S, XU K, LIU X LIU. Experimental study of Chinese ink as a new type of dye tracer in sentinel lymph node biopsy. *Chin Germ J Clin Oncol*. 2006;5(1):36–39. doi:10.1007/s10330-005-0434-1
22. Mori K. Identification of lymphatic vessels after intra-arterial injection of dyes and other substances. *Microvasc Res*. 1969;1(3):268–274. doi:10.1016/0026-2862(69)90029-6
23. Kato S, Shirai Y, Sakamoto M, Mori S, Kodama T. Use of a lymphatic drug delivery system and sonoporation to target malignant metastatic breast cancer cells proliferating in the marginal sinuses. *Sci Rep*. 2019;9(1):13242. doi:10.1038/s41598-019-49386-5
24. Bouta EM, Wood RW, Perry SW, et al. Measuring intranodal pressure and lymph viscosity to elucidate mechanisms of arthritic flare and therapeutic outcomes. *Ann N Y Acad Sci*. 2011;1240:47–52. doi:10.1111/j.1749-6632.2011.06237.x
25. Kato S, Takeda K, Sukhbaatar A, et al. Intranodal pressure of a metastatic lymph node reflects the response to lymphatic drug delivery system. *Cancer Sci*. 2020;111(11):4232–4241. doi:10.1111/cas.14640
26. Miura Y, Mikada M, Ouchi T, et al. Early diagnosis of lymph node metastasis: importance of intranodal pressures. *Cancer Sci*. 2016;107 (3):224–232. doi:10.1111/cas.12873
27. Rohner NA, McClain J, Tuell SL, et al. Lymph node biophysical remodeling is associated with melanoma lymphatic drainage. *FASEB J*. 2015;29 (11):4512–4522. doi:10.1096/fj.15-274761
28. Vo A, Doumit M, Rockwell G. The biomechanics and optimization of the needle-syringe system for injecting triamcinolone acetonide into keloids. *J Med Eng*. 2016;2016:5162394. doi:10.1155/2016/5162394
29. Jacob L, de Brito Neto J, Lenck S, et al. Conserved meningeal lymphatic drainage circuits in mice and humans. *J Exp Med*. 2022;219(8). doi:10.1084/jem.20220035
30. McCright J, Skeen C, Yarmovsky J, Maisel K. Nanoparticles with dense poly(ethylene glycol) coatings with near neutral charge are maximally transported across lymphatics and to the lymph nodes. *Acta Biomater*. 2022;145:146–158. doi:10.1016/j.actbio.2022.03.054
31. Oshiro H, Osaka Y, Tachibana S, Aoki T, Tsuchiya T, Nagao T. Retrograde Lymphatic Spread of Esophageal Cancer: a Case Report. *Medicine*. 2015;94(27):e1139. doi:10.1097/MD.0000000000001139
32. Joshi AS, Singh V, Gahane A, Thakur AK. Biodegradable nanoparticles containing mechanism based peptide inhibitors reduce polyglutamine aggregation in cell models and alleviate motor symptoms in a drosophila model of huntington's disease. *ACS Chem Neurosci*. 2019;10 (3):1603–1614. doi:10.1021/acschemneuro.8b00545
33. Dominy SS, Lynch C, Ermini F, et al. Porphyromonas gingivalis in Alzheimer's disease brains: evidence for disease causation and treatment with small-molecule inhibitors. *Sci Adv*. 2019;5(1):eaau3333. doi:10.1126/sciadv.aau3333
34. Ahmadi Badi S, Moshiri A, Fateh A, et al. Microbiota-derived extracellular vesicles as new systemic regulators. *Front Microbiol*. 2017;8:1610. doi:10.3389/fmicb.2017.01610